


ORIGINAL ARTICLE

Experimental measurement of initial evaporation mass flows from gasoline spills and comparison with empirical models

Ronald Zinke¹  | Naresh Virothi¹ | Florian Köhler¹ | Andrea Klippel¹ | Sebastian Schalau² | Ulrich Krause¹

¹Department of Plant Design and Process Safety, Otto-von-Guericke University Magdeburg, Magdeburg, Germany

²Bundesanstalt für Materialforschung und -prüfung (BAM), Berlin, Germany

Correspondence

Ronald Zinke, Otto-von-Guericke University Magdeburg, Department of Plant Design and Process Safety, Universitätsplatz 2, Magdeburg 39106, Germany.
Email: ronald.zinke@ovgu.de

Funding information

University of Hamburg

Abstract

In this paper, we investigate the evaporation mass flow originating from spills of gasoline. Large spills of gasoline may form during partial or complete roof sinkings or in the case of perforations at various deck fittings at external floating roof tanks used for the storage. Additionally, spills may form in the retention area in the case of leakages at pipes or at the hull. The aim is to predict the order of magnitude of real-scale evaporation mass flow. The determined evaporation mass flows will be used in a related project as input values for subsequent dispersion modeling in the vicinity of the tanks. This is relevant for questions of fire and explosion protection as well as for environmental protection aspects in tank farms or refineries, which use external floating roof tanks. The measurements presented in this paper were compared with predictions by empirical models and investigations of evaporations from small floor spills, round-bottom flask, or from Petri dishes published in the literature. The main goal of this paper is to test the applicability of empirical models to provide reasonable evaporation mass flows as input for CFD dispersion simulations.

KEYWORDS

evaporation mass flow, external floating roof tanks, gasoline spills, spill evaporation

1 | INTRODUCTION

In refineries or tank farms, large amounts of crude oil and derived petroleum products are stored temporarily before transport, typically in suitable storage tanks, for example, in fixed-roof or external floating-roof tanks (EFRT). Fixed roof tanks, which are mandatory for compounds with very high vapor pressure or with a high-risk potential (toxicity), are characterized by having an immovable roof above the tank cylinder. They are also typically connected to a gas collection line.

In contrast to a fixed-roof, a floating-roof is lifted or lowered depending on filling or withdrawal procedures and floats effectively on the stored liquid.

External floating-roof tanks, which are considered in this project, have no additional fixed roof to cover the tank cylinder from the environment in contrast to some fixed roof tanks, which may also have an internal floating roof for emission reduction.

As stated earlier, the decision whether to use a fixed-roof or an EFRT depends (among other points) on the vapor pressure of the storage liquid or its hazard class and is usually regulated, cf. in the EU.¹

The main consequence of the differences in the construction is that fixed roof tanks can be operated in such a way that there are no direct emissions of product vapors into the environment. Nevertheless, due to the operation of the gas treatment they are structurally more complex and thus cause indirect emissions and have additional

This is an open access article under the terms of the Creative Commons Attribution-NonCommercial License, which permits use, distribution and reproduction in any medium, provided the original work is properly cited and is not used for commercial purposes.

© 2019 The Authors. *Process Safety Progress* published by Wiley Periodicals, Inc. on behalf of American Institute of Chemical Engineers.

risk potential.² More detailed information can be found for example, in References 3-5.

1.1 | Project motivation

The results to be presented in this publication are embedded in a parent project. In this parent project, the main focus is on emissions from EFRT in normal operations as well as in deviations from normal operation such as damages or faulty operation. From a physical point of view, the tanks are not closed systems, thus emissions of volatile organic compounds (VOCs), have to be expected in principle. Because of the flammability of VOCs, also certain likelihood for the formation of ignitable concentrations of flammable gases has to be taken into account. In a previous project,^{6,7} the emission behavior of a representative EFRT storing gasoline during normal operation was estimated using the API 2517/19⁴ and experimentally controlled within a long-term measurement. The focus was on the relevance of the emissions on explosion protection and particularly in lightning protection for the retention area. During the long-term measurement, no ignitable concentrations of VOCs were detected but concentrations within one and two digit ppm values absolute. Thus, the formation of ignitable concentrations of VOCs, especially in the retention area, is unlikely in normal operation.⁶

1.2 | Actual project: scope and strategy

Related to the probability of the occurrence of an ignitable concentration of VOCs is the zone assignment to the hazardous area. A specific zone classification is to be justified in the context of a risk assessment, which ensures the interests of explosion protection. Here, it was decided to include deviations from normal operation as revision procedures but also various damages to emission-relevant components. For recording emission relevant damages, a literature survey, a Germany-wide survey of companies that use EFRT, and an expert survey were carried out. Next, a risk assessment based on Bayesian networks was made.

The overall aim of the ongoing project is to find out events and probabilities, which may cause the formation of ignitable concentrations of VOCs above the roof and next to the tank in the retention.

Estimates of emission mass flows are carried out using the API 2517/19 for revisions but are based on novel approaches in case of damages, since no precise models are available in the literature. The dispersion of VOCs is investigated by CFD simulations which are supported by investigating the flow around the tank using a representative model in a wind tunnel. The CFD simulations are designed to show whether emissions from the roof can lead to a hazard in the retention area and give information about the spatial extension of the emission.

The estimates of the mass flow resulting from damage investigations clearly show that spills of refinery products having a high vapor pressure as for example, gasoline or naphtha are sources for dangerous emissions. These spills can form in the case of partial or complete roof sinking, in the case of various rust damages to deck fittings or in

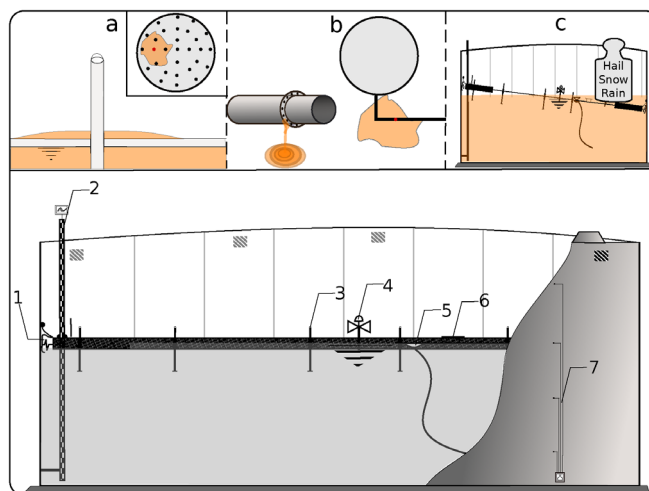


FIGURE 1 Illustration of an EFRT equipped with typical deck fittings. 1: rim seal, 2: guide pole, 3: deck leg, 4: vacuum breaker, 5: deck drain, 6: access hatch, and 7: sampling. Typical locations for potential spill formations: a, b, and c. EFRT, external floating-roof tank [Color figure can be viewed at wileyonlinelibrary.com]

case of leakage at the tank hull or the pipes in the retention area. An illustration of a typical EFRT and locations of potential spill formations are shown in Figure 1. As this project is still in progress, this publication does only contain investigations related to evaporation mass flows of gasoline from spills. The other project parts will be published in the near future.

1.3 | Spill formation and evaporation models

If a fluid is released in the case of an accident, many factors influence further whereabouts. Relevant influential conditions for the leaking fluid are physical boundary conditions such as temperature, pressure liquefaction, ambient conditions, partial evaporation and/or spill formation. When forming a spill, the confinement, a minimum layer height, seeping into the ground, adhesion, porosity, ground topography and many other influences are present. The location of the spill itself, such as sink, a flushfloor situation or a hill can be present. Even a film on another liquid is conceivable. Typically, both the formation and the disappearance of spills are highly dynamic processes, of which not all can be considered in a single model that remains also practically applicable. In the literature, no models are found, which completely describe fully dynamic the formation and disappearance processes in a nontrivial simulation (CFD-model).

For simplifications, it is therefore often assumed that the formation processes can be neglected, as if it happens instantaneously. Also, one has to realize that in advance many of the conditions necessary for an accurate prediction cannot be specified. Therefore, one often cannot benefit from the supposedly more accurate model. For the resulting spill, one often assumes additionally a well-defined stationary geometry on a plane flushfloor surface. The disappearance of the spill happens by boiling or evaporation, but only the case of evaporation will be considered here.

Models available in the literature can be divided into two basic groups: (a) stationary models such as simplified boundary layer models and empirical/semi empirical models (including film theory) and (b) non-stationary models such as boundary layer models (CFD) or energy balance models.

Boundary layer models usually provide a system of partial differential equations for the boundary layer fields temperature $T(\vec{x}, t)$, pressure $p(\vec{x}, t)$, and velocity $\vec{u}(\vec{x}, t)$ with the aim to determine a transfer coefficient β (dimension: $[\beta] = LT^{-1}$, $\beta = \frac{Sh \cdot D}{L}$, Sh: Sherwood-number, T , L time, length-dimension, and D molecular diffusivity) and finally to determine the mass loss $\dot{m}(t)$ ⁸. This is generally treated numerically. In principle, multiple influences can be taken into account through additional balance equations. Energy balance models, for example, Reference 8 accounts for all significant energy transfers entering and leaving the spill. Since typically all involved temperatures (spill, ambient air, and ground) are time depending ($T = T(t)$) also all energy transfers are explicitly dynamic. Usually radiation energy fluxes (\dot{q}_{rad}), energy fluxes due to incoming substance \dot{q}_{in} , evaporation \dot{q}_{evap} and energy transport into the ground \dot{q}_g are taken into account and modeled within a balance equation for $\dot{m}(t)$.

Empirical models attempt to describe the evaporation of the spill to the air layer above by a transfer coefficient β , which includes both material characteristics and the turbulent properties of the air flow. This usually leads directly to empirical equations, for example, References 9-11 for β or advection diffusion equations for which analytic expressions for $\dot{m}(t)$ ¹² can be found (for simple spill geometries) as for example, References 12-14.

In this work and also for the overall project, it was decided to test the applicability of empirical models. This is due to the fact that for the energy balance models and especially for the CFD models very precise conditions must be defined so that a benefit from their inherent higher accuracy can be expected.

1.4 | Evaporation of gasoline spills

There are some papers published to the investigation of gasoline spill evaporation.¹⁵⁻²¹ The evaporation is empirically described there mainly by adaptation of a mass transfer coefficient. In contrast to substances such as water or pure short-chain alkanes, mixtures of substances such as gasoline show deviating evaporation behavior. During the evaporation process, the composition changes as the more volatile components dominate the initial phase of evaporation,¹⁷ and as a result, the overall dynamics of the evaporation changes significantly in time.^{15,16} It is therefore clearly pointed out in Reference 16 that evaporations from gasoline spills, and especially from crude oil spills follow another dynamic, as can be expected in accordance with boundary layer related empirical models (cf. also Section 2). For example, the evaporation rate depends on surface and flow velocity but not in the same way as predicted for pure substances, and the mass loss is not constant, but decreases exponentially with time or, respectively, the evaporated fraction shows a logarithmic time dependence. In the previously cited papers, it was therefore investigated as to how the

composition and physical parameters, such as vapor pressure and viscosity, change during the evaporation^{15,18} or how the long-term evaporation after blending with ETBE¹⁹ is influenced. Also, vertical diffusion during the evaporation process and concentration profiles was considered more closely.²⁰

In the cited literature, however, small spills on a floor or small liquid surfaces on Petri dishes or in round bottom flasks were considered. However, no equations are given which allow the estimate of \dot{m} ¹⁵ right after the spill formation. The formula from Reference 15 cannot be applied for periods less than 1 day because a logarithmic term in the equation would predict negative weight decreases. In Reference 18, no wind was taken into account, therefore there are no flow influences but only diffusive transport. The extensive work of Reference 16 considers very precisely the evaporation behavior of different oils but gives no estimates of \dot{m} for gasoline concerning the demand of the actual project. The papers have more or less in common that the long-term evaporation behavior is in the foreground and not the order of magnitude shortly after spill formation.

More extensive gasoline spills on concrete, as they may occur at petrol stations, were investigated theoretically in Reference 21. There an empirical model, originally made for describing water evaporation was modified for estimating gasoline evaporations.

In Reference 21, the evaporation mass flow is converted to a liquid level decrease assuming a constant spill surface. For these calculations, the change in mixture composition and the consequences on the evaporation rate were not taken into account. In addition, the reciprocal of the psychrometric constants was erroneously used there, so the predicted level decreases are not correct. If one compares the evaporation mass flows of Reference 15 with those of Reference 20, there are also differences that are not within the uncertainty of the material parameters. Also, no explicit comparisons are made with other empirical models available in the literature.

In the present paper, the evaporation mass flow in the initial phase after the formation of the spills are to be estimated, not the precise influence of composition changes. It will be experimentally tested whether simple empirical models (which are also easy to use) can provide sufficiently accurate predictions of \dot{m} for subsequent CFD simulations in case of accident events.

1.5 | Organization of the paper

In Section 2, some empirical spill evaporation models are briefly presented. Model comparisons are made and statements for model validity are given. It will also be discussed to what extent the empirical models are suitable for describing evaporation mass flows of gasoline or refinery products of comparable high vapor pressure.

For the experimental measurement of evaporation mass flows, experimental spills were produced in an open-air test area. For this purpose, liquid surfaces were produced in cylindrical steel containers. The composition of the spills and the experimental setup for recording the evaporation mass flow as well as the environmental conditions required for the empirical models are described in Section 3.

Section 4 compares the experimentally measured data with model predictions and literature data (if available). Deviations between model predictions and experiments are discussed and the expected order of magnitude of the evaporation mass flow is estimated for realistic spill sizes on EFRT or next to them in the retention. In Section 5, the paper will be summarized.

2 | EMPIRICAL SPILL EVAPORATION MODELS

Empirical spill evaporation models assume that the spill forms a level with the ground without additional flow obstacles; the spill has a well-defined shape and considers stationary evaporation only. In this case, neither the spatial dimensions of the spill, nor the physical parameters such as temperature, the wind speed, and direction or the composition change. In our case, the liquid surface in a container actually violates the condition of a plane spill at the ground-level. In Reference 9, it was shown that this can actually have an effect on the mass loss, but does not necessarily change the order of magnitude. In addition, true stationary conditions will never actually exist because the environmental conditions will change in the periods relevant to the accident scenarios at EFTR. Therefore, the goal should be reminded once again whether a fundamental estimate of the mass loss with empirical models makes sense here. An overview of spill evaporation models can be found for example, in References 16 and 22

Among the published empirical spill evaporation models for further consideration the models of Sutton and Pasquill^{12,13} and the model of Deutsch⁹ will be used. Frequently cited models (cf. Reference 22) of Mackay-Matsugu and Clancey^{10,11} are derived from the model of Sutton and Pasquill. However, Mackay-Matsugu¹¹ has only modified the mass transfer coefficient, while Clancey¹⁰ derives a dimensionally incorrect model because a viscosity-dependent factor was added due to a misunderstanding. The model of Mackay-Matsugu also has the problem that because of the profile exponent at the wind velocity, a decrease in mass transport is predicted with increasing profile exponents, although the ground turbulence increases.⁹ According to the model of Sutton and Pasquill, the evaporation mass flow for a circular spill can be estimated under the conditions given earlier with:

$$\dot{m} = 0.0824 \frac{p_d M}{RT} u^{\frac{7}{9}} r^{\frac{17}{9}} D^{\frac{2}{3}} z^{-\frac{1}{3}}. \quad (1)$$

Here, D is a molecular diffusivity to describe the mass transfer into the air, u is the overflowing wind velocity in height z over the spill, T is the spill temperature, M is the molar mass of the vaporizing substance, p_d its vapor pressure (at T of the spilled liquid), and R is the universal gas constant. It is further assumed that the spill is circular with radius r .

For the model of Deutsch, in principle, the same assumptions were made. Instead of a radius, the surface of the spill A and the expansion of the spill in wind direction r_L is needed.

According to the model of Deutsch, the evaporation can be estimated to:

$$\dot{m} = 0.077 \alpha^{0.156} Re^{0.76} Sc^{0.19} \frac{DMAp}{RT r_L} \ln \left(\frac{p}{p - p_d} \right). \quad (2)$$

Here, $Re = \frac{ur_L}{\nu}$ is the Reynolds number for $u = u(z = 10 \text{ m})$, p is the ambient pressure, $Sc = \frac{\nu}{D}$ is the Schmidt number depending on D , and the kinematic viscosity of the ambient air ν and α is a profile factor to account for different turbulence spectra near the ground caused by different soil conditions (roughness lengths). For α , the following values are used depending on the roughness: $\alpha = 0.08$ - 0.12 (smooth), $\alpha = 0.13$ - 0.18 (moderately rough), $\alpha = 0.20$ - 0.24 (rough), and $\alpha = 0.28$ - 0.40 (very rough).

According to (1) and (2), the higher the vapor pressure and the mass transfer coefficient, the higher the evaporation mass flow, given the same size of the spill and the same ambient conditions.

In Reference 23, D was experimentally determined for various gasoline fuels (91, 95, and 98 octane, as well as for mixtures thereof). It could be shown that with increasing octane number the diffusion coefficient decreases and for $T = 323 \text{ K}$ (50°C) in the range of $D \in [7.4 \cdot 10^{-7} \text{ m}^2 \text{ s}^{-1}; 2.1 \cdot 10^{-6} \text{ m}^2 \text{ s}^{-1}]$. The highest value was determined for a mixture of petrol and ethanol (grade: UAE gasoline E+). If this fuel grade is removed, D is in the range of $D \in [6.4 \cdot 10^{-7} \text{ m}^2 \text{ s}^{-1}; 7.4 \cdot 10^{-7} \text{ m}^2 \text{ s}^{-1}]$. The temperature dependence of binary diffusion coefficients can be described approximately⁹ by a power law:

$$D(T) = D(T_0) \left(\frac{T}{T_0} \right)^{1.5}. \quad (3)$$

With $T = 323 \text{ K}$ and $T_0 = 293 \text{ K}$, it can be found for the diffusivity $D(T_0) \approx 0.86D(T)$. This means that D does not decrease significantly in this temperature range. In this work, $D = (7.0 \pm 0.5) \times 10^{-7} \text{ m}^2 \text{ s}^{-1}$ will be used, since it can be considered conservative for lower temperatures.

The model of Deutsch requires the dynamic viscosity of air. In Reference 24, $\nu = 15 \times 10^{-6} \text{ m}^2 \text{ s}^{-1}$ at $T = 293 \text{ K}$ is specified and will be used here without additional errors.

The vapor pressure of gasoline is highly temperature-dependent. Furthermore, it depends on the blend and also varies considerably between different refineries.²⁵ As a rule, these product-related fluctuations are well above the uncertainties of the vapor pressure determination methods. Usually, however, at least Reid vapor pressures²⁶ are known. For converting the vapor pressure to other temperatures, the Clausius-Clapeyron equation can be used. In the API 2517/19,⁴ also the Antoine equation derived from the latter one is applied:

$$p_d(T) = e^{A - \left(\frac{B}{T+C}\right)}. \quad (4)$$

Here, A , B , and C represent parameters which are determined by curve fitting for the different mineral oil products. They depend on the slope S of the distillation curves at 10% evaporation according to

ASTM D86.²⁷ These formulas will be cited here but converted to (derived) SI-units (Pascal, Kelvin):

$$\frac{p_d(T)}{6894.76} = \exp \left\{ \left\{ 0.33 - \frac{99.65}{T} \sqrt{S} \ln(p_r) \right. \right. \\ \left. \left. - 4.75 \sqrt{S} + \frac{1459.62}{T} \sqrt{S} \right. \right. \\ \left. \left. + \left(\frac{582.92}{T} - 0.87 \right) \ln(p_r) \right. \right. \\ \left. \left. - \frac{10008.81}{T} + 23.37 \right\} \right\}. \quad (5)$$

In API 2517/19, *S* guideline values are suggested if there is no corresponding distillation data. One finds the value *S* = 3.0 for gasoline. Note that p_r is the Reid vapor pressure.

For a temperature of $T = 293$ K the ranges for Reid vapor pressure given in DIN EN 228²⁸ will result in a range of $p_r = 26$ kPa to 36 kPa for summer blend and to a range of $p_r = 36$ kPa to 55 kPa for winter blend. Here, conservatively $p_d = (45 \pm 10) \times 10^3$ Pa will be used at $T \approx 293$ K.

In Reference 29, a mean value of $M = 99$ g mol⁻¹ was given for the molar mass of gasoline. In Reference 30, a value of $M = 95$ g mol⁻¹ can be found. In Reference 31, a range of $M = 80$ g mol⁻¹ to $M = 110$ g mol⁻¹ is given. Summarizing $M = (0.095 \pm 0.015)$ kg mol⁻¹ for the molar mass can be derived.

For the conversion of the evaporation mass flow into an effective level, decrease in the density of gasoline is needed. The fuel density varies with the composition and the blend. The maximum allowable density of the blend is $\rho_{\max} = 775$ kg m⁻³, the minimum allowed density is $\rho_{\min} = 720$ kg m⁻³ (limit values according to DIN EN 228). For this work, a value of $\rho = (750 \pm 30)$ kg m⁻³ is used.

Both models require the specification of the wind speed at a reference altitude. In the model of Deutsch, the reference height is $z = 10$ m. A conversion of the wind speed to other heights can be done with the previously specified profile factor α :

$$u(z_1) = u(z_0) \left(\frac{z_1}{z_0} \right)^\alpha. \quad (6)$$

Because the inflow was in the wake of some research buildings, a value of $\alpha = 0.25$ was chosen. Furthermore, it is assumed that the heat dissipation associated with the mass flow rates of evaporation does not lower the spill temperature. Since the evaporation mass flow decreases with decreasing spill temperature, this assumption is again conservative with respect to the evaporation mass flow.

3 | EXPERIMENTAL SETUP AND MEASUREMENTS

For the experimental measurement of the evaporation mass flows $\dot{m}(t)$, steel cylinders with different radii ($r = 0.1$ m, 0.2 m, 0.3 m, and 0.75 m) and a common height of $h = 0.3$ m were filled. These steel cylinders, except the largest one, were positioned on scales (Kern Balance³²) with a resolution of ± 0.5 g that recorded the mass loss due to evaporation.

The test substances were winter and summer blends of commercial super gasoline (RON 95) from a petrol station. The cylinders were filled to the same level in each experiment. Basically, there was always a height gap of 0.25 m to the upper edge of the cylinder at the beginning of every experiment. The cylinder with a radius of 0.75 m was floated on a water bath inside a larger cylinder. IR detectors were placed around the cylinder filled with water to determine the concentration of volatile organic hydrocarbons. The float tank was filled with gasoline (summer blend) to a level of 0.05 m. Also here, a height gap of 0.25 m between the water level and the upper edge of the (larger) cylinder was present at the beginning of the experiment.

The temperature T_l of the liquid and the ambient temperature T_a were recorded continuously with two thermocouples (resolution: ± 0.1 K) each. Additionally the wind speed $u(t)$ (absolute value) was continuously measured at a height of 1 m above the surface of the spill with an ultrasonic anemometer (METEK-USA-I-CHT,³³ resolution: $u(t) > 0.1$ m s⁻¹, ± 0.01 m s⁻¹). A schematic overview of the experimental set-up is shown in Figure 2. For the experiments the determination of mass flow rates in the beginning of the evaporation are of particular interest. It is also important to keep in mind that the measurements were subjected to evaporation-influencing factors such as wind speed and temperature fluctuations. Again, it is therefore stated here that the determined mass losses represent orders of magnitude (orientation values) only. The experiments were carried out in the open air in winter and summer. As a test site, an area at the Institute of the fire brigade³⁴ was used, where there are large open concrete areas for fire tests.

3.1 | Experiment No. 1: Comparison of winter and summer blend

In this experiment, winter- and summer blends were filled into the small cylinder (radius $r = 0.10$ m). The measurement using the winter blend had been done in March at a sunny day (neutral atmosphere)

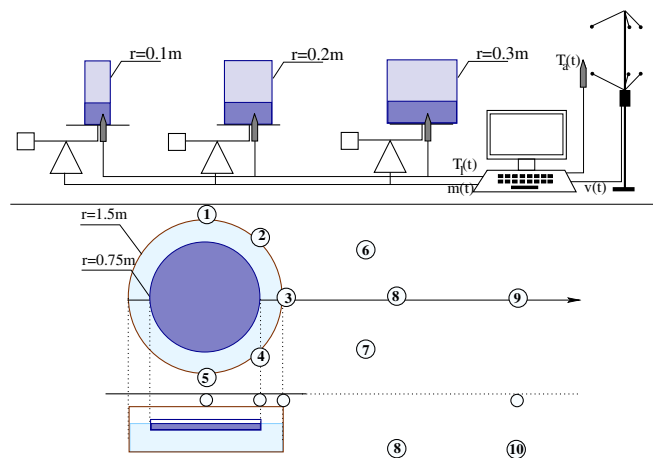


FIGURE 2 Illustration of the experimental set-up of the spill evaporation measurements. For the detector 3, later concentration measurements are shown [Color figure can be viewed at wileyonlinelibrary.com]

with an average ambient temperature of $\vartheta_a = 10^\circ$, while the test with the summer blend was done in July with $\vartheta_a = 24^\circ$ (neutral atmosphere). The vessels were positioned such that there was no direct sunlight on the liquid. At the beginning of the experiments, the material temperatures were close to the ambient temperatures. The mass loss as a function of time is shown in Figure 3 (top: winter blend, bottom: summer blend). It can be seen from the figure that for both blends the initial mass loss of evaporation has a maximum at the beginning and then drops gradually. The linear fits give an indication of the order of magnitude of \dot{m} in the beginning.

Here, the 100-second averages were determined to 0.19 g s^{-1} for winter blend and, respectively, 0.25 g s^{-1} for summer blend. Within these periods, both the liquid composition and the temperature change. The composition changes due to the preferred evaporation of the volatile components and the temperature changes due to the energy loss (heat of evaporation), so that there is no stationary state. The indicated mean values nevertheless give a representative

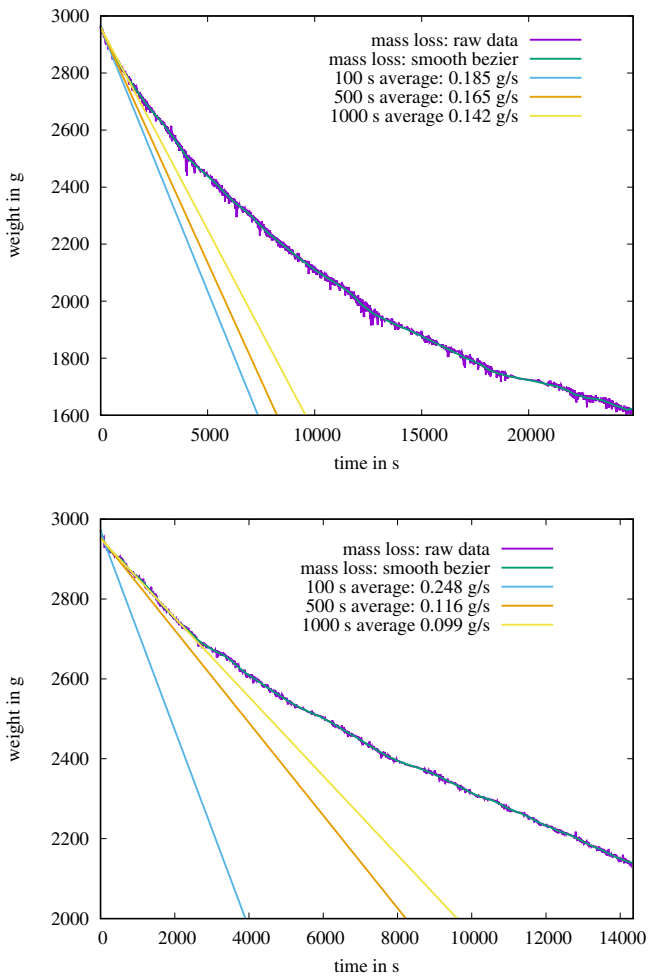


FIGURE 3 Illustration of the weight depending on the time for winter blend (top; date: 03.2019) and summer blend (bottom; date: 07.2019). The raw data and smoothed curves using Bezier curves are shown. The linear functions are fit functions including the weight for the first 100, 200, and 500 seconds [Color figure can be viewed at wileyonlinelibrary.com]

order of magnitude for the mass loss of the evaporation with respect to the present ambient condition.

For the experiment using the winter blend, the liquid and ambient temperature depending on the time were represented in Figure 4. It can be seen a significant decrease in the liquid temperature within the first 2500 seconds and then a certain correlation with the ambient temperature. This correlation is only due to the small total amount of gasoline and is not expected at an EFRT in case of partially or completely sunken roofs. The wind speed (not illustrated) fluctuates strongly near the ground in between 0 m s^{-1} and 4 m s^{-1} , with a mean value of about 1.2 m s^{-1} . The full value range of the measured wind speeds cannot be used for specifying wind fluctuations since short-term peaks have no influence on the evaporation. As an error estimate, an orientation can be made to the deviations given by the Bezier curve (cf., eg, Figure 7) from the mean value. Here, $u = (1.2 \pm 0.5) \text{ m s}^{-1}$ seems plausible and will be used for uncertainty investigations.

3.2 | Experiment No. 2: Surface dependence of initial gasoline evaporation

For this series of evaporation experiments, three containers of different radii were used to investigate the influence of the surface in the open air case. The measurements took place simultaneously (also simultaneously to experiment no. 3 below), so that all vessels were subjected to nearly the same environmental conditions. Again, all vessels were filled to the same height of 0.05 m in the beginning. The corresponding mass losses are shown in Figure 5. For the purpose of a better comparison, the starting mass was subtracted from the current value, so that all curves start at zero. The straight lines that are displayed provide a fit using the data of the first 500 seconds. This

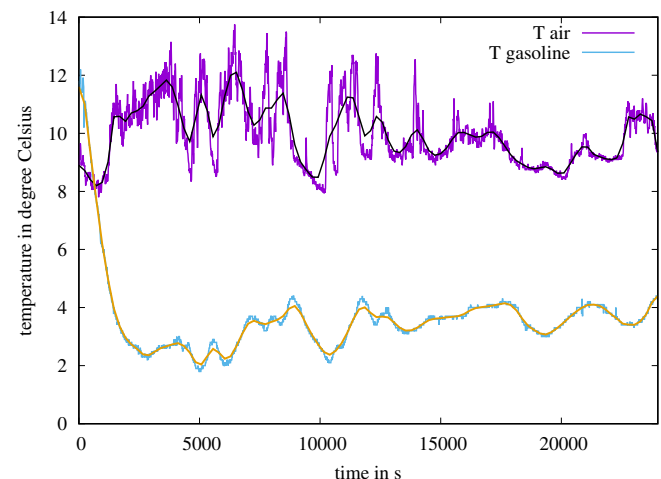


FIGURE 4 Illustration of the liquid and ambient temperature depending on the time. Here, the data from the experiment using the winter blend are shown. The curve smoothing was again performed with Bezier curves (not labeled) [Color figure can be viewed at wileyonlinelibrary.com]

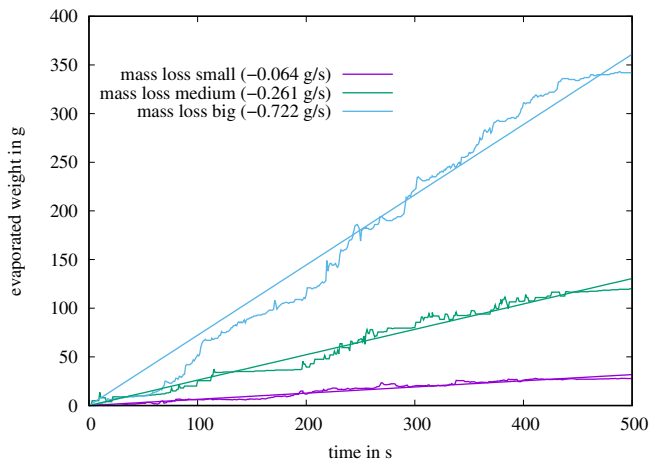


FIGURE 5 Illustration of the evaporated weight of gasoline (summer blend) from vessels with different radii under open air (magenta: $r = 0.1$ m, green: $r = 0.2$ m, and blue: $r = 0.3$ m) [Color figure can be viewed at wileyonlinelibrary.com]

slightly longer time interval has been chosen because the turbulent wind causes larger fluctuations in the balance display, especially for the larger vessels. It can be seen from Figure 5 that there is a strong correlation between the mass loss and the surface. According to the empirical models, \dot{m} is proportional to $A^{1/2}$ (Sutton-Pasquill) or proportional to $A^{0.88}$ (Deutsch). With the studies conducted here, it is not possible to check precisely if the measured values support the expectation. That is because the accuracy of the experiments is not sufficient. Furthermore, the position of the spill in the interior of a cylinder actually violates the model assumptions of the empirical models. Nevertheless, in the transition from the middle ($r = 0.2$ m) to the large container ($r = 0.3$ m), the area increases with a factor of 2.25. According to the models, the mass flow should then increase with a factor of approximately 2.1. The measured values show a factor of 2.7 (see Figure 5).

3.3 | Experiment No. 3: Open-air evaporation of gasoline (large vessel)

In experiment no. 3 with the largest cylinder, a floating roof tank situation was modeled. For this purpose, a large steel container was filled with water, on which the test cylinder floats. The level loss on the ruler was read off at regular intervals of about 5 minutes. The corresponding mass loss was calculated using the gasoline density given in the previous section. The water here serves as a warm bath, which should reduce temperature fluctuations during the gasoline evaporation. The setup of the experiment is shown in Figure 2. The mass loss depending on the time is shown in Figure 6. Since only a few data points were available, the tolerances for the mass loss are higher than in the previous experiments, but with high confidence within 2.5 g s^{-1} to 4.5 g s^{-1} with an average of 3.5 g s^{-1} including the deviations of the density. For a comparison with the empirical models, a mean spill temperature and an average wind speed are needed. The

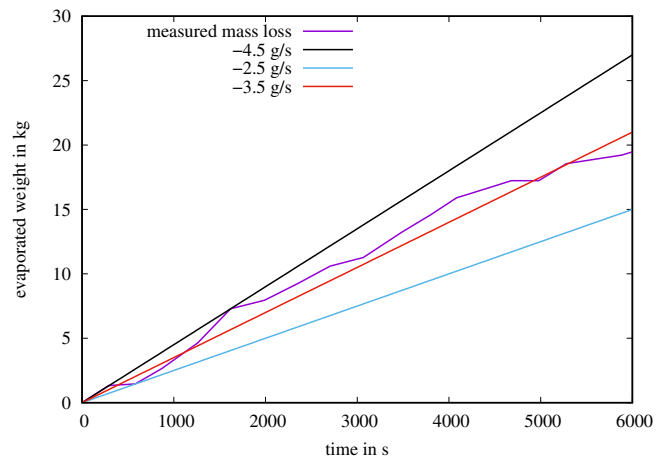


FIGURE 6 The mass loss depending on the time for the evaporation of gasoline from the floating test cylinder. Here, an average mass loss as well as a lower/upper linear approximation is shown [Color figure can be viewed at wileyonlinelibrary.com]

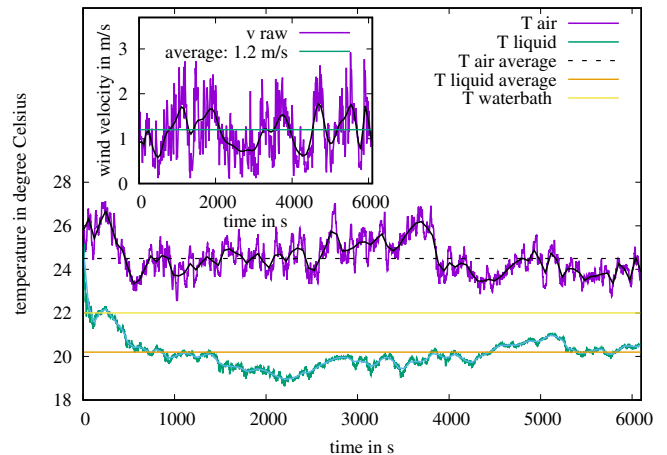


FIGURE 7 The temperatures (liquid and environment) and the wind speed depending on the time for the evaporation of gasoline from the floating test cylinder [Color figure can be viewed at wileyonlinelibrary.com]

time dependence of the measured temperatures (liquid and environment) and the wind speed are shown in Figure 7. Because of the water bath, the change in the temperature of the liquid is less pronounced than in the experiment with the small cylinder. First, the temperature drops due to the heat of evaporation. The initial temperatures of the water bath and the gasoline are about the same at 26°C . In the further course of the experiment, the gasoline remains slightly colder than the water bath and the fluctuations are also slightly lower compared to the experiment with the small cylinder. This was to be expected and is a consequence of the effect of the water bath which dampens temperature fluctuations in the gasoline by heat transport.

The value $T_l = (293 \pm 2)\text{K}$ was determined as suitable average value and fluctuation for the spill temperature. For the wind speed, again a value of $u = (1.2 \pm 0.5) \text{ m s}^{-1}$ of the approximately two-hour

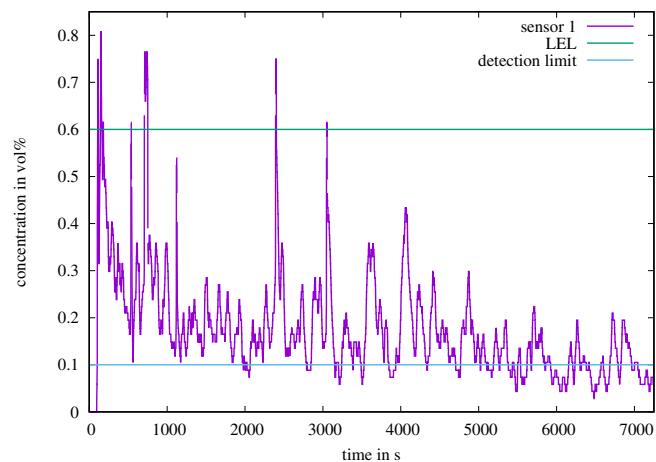


FIGURE 8 Measurement of airborne concentrations of VOCs in the vicinity of the tank at the detector position 3 (see inset and cf. Figure 2). VOC, volatile organic compound [Color figure can be viewed at wileyonlinelibrary.com]

measurement was estimated. A special feature of this experiment was that 10 IR-detectors (SMART IR EX³⁵) were used to measure the concentration of VOCs in the ambient air at different positions (cf. Figure 2) around the large test vessel. This should measure how often the LEL is exceeded at the level of the upper edges of the water-filled cylinder and at a slightly greater distance (in the mean wind direction).

Laboratory investigation done for the project⁶ shows that the IR-detectors used are suitable for detecting gasoline vapors with concentrations above several hundred parts per million. The IR absorption bands are quite similar for the individual compounds contained in gasoline, so that a calibration factor can also be found for the mixture. However, the IR detectors operate in diffusion mode, thus having quite large response times and tending to attenuate the peaks of fluctuating signals. It is possible that a short-term exceed of the LEL, caused by turbulent fluctuations, is not detected due to the sensor's response time.

Within the large cylinder, and in particular in the immediate vicinity of the floating tank with the gasoline, the detectors measure concentrations far above the LEL (not shown) but the concentrations decrease very rapidly with increasing distance. The detectors in positions 1-5 (see Figure 2) show concentrations predominantly between 1000-3000 ppm, but there is a recurrent reaching and exceeding of the LEL. Figure 8 shows the recorded concentration profile of the detector at position 3. It can also be seen from this image that the frequency of detected high peaks decreases over time. The detectors 1 and 2 as well as 4 and 5 show similar behavior. By contrast, the other detectors only show noise below the detection limit (not illustrated). None of the detectors on the ground showed a peak reaching beyond the detection limit of 1000 ppm. For a real tank situation, however, it must be assumed that depression of vortices of higher VOC concentrations is possible in the downstream flow of the tank.

For EFRT, it can be concluded that spills on the roof can well lead to concentration profiles above the LEL on the roof and in the close vicinity to the tank. Also within the retention area concentrations

above the LEL seem plausible. In both the cases, however, the spills must not be too small. Otherwise, there may be no hazardous explosive atmosphere because the total amount of flammable gas is too low.

4 | RESULTS AND DISCUSSION

First, the mass flows calculated with the empirical models are to be given and discussed. The minus sign of the mass loss will be omitted here. The expected values and the fluctuations for the mass loss were calculated according to the empirical models with the material data given in Section 2. The specified fluctuations were calculated from the expected values, the material data and their fluctuations using the total error differential. Here, the specified fluctuations of the molar mass, the density, the vapor pressure, the temperature, the wind speed and molecular diffusivity were taken into account. The individual contributions to the model uncertainties are not explicitly stated here. Nevertheless, the large fluctuations in the empirical models are primarily from the high uncertainties regarding vapor pressure and wind speed. Less pronounced is the influence of uncertainty in the temperature of the spill.

For experiment no. 3 the model of Sutton-Pasquill predicts a mass loss of $(4.0 \pm 3.0) \text{ g s}^{-1}$. Despite the high experimental uncertainties, this range is in the same order of magnitude compared with the measured results of $(3.5 \pm 1.0) \text{ g s}^{-1}$, which are shown in Figure 6.

For the tests with the other cylinders within the experiment no. 1 and 2, the expectation values and fluctuations according to the model of Sutton-Pasquill are in the ranges $(0.09 \pm 0.07) \text{ g s}^{-1}$ ($r = 0.1 \text{ m}$), $(0.33 \pm 0.24) \text{ g s}^{-1}$ ($r = 0.2 \text{ m}$), and $(0.71 \pm 0.52) \text{ g s}^{-1}$ ($r = 0.3 \text{ m}$). For these experiments, too, one finds a useful match for the order of magnitude of \dot{m} with the results of the measurements (which are given in Figure 5). Next, the results obtained by the model of Deutsch will be discussed. The model of Deutsch generally predicts smaller values for the evaporation mass flow. For the experiment no. 3 (vessel with the radius of $r = 0.75 \text{ m}$) a value of $(2.4 \pm 2.0) \text{ g s}^{-1}$ is found.

For the tests with the other cylinders the values $(0.07 \pm 0.60) \text{ g s}^{-1}$ ($r = 0.1 \text{ m}$), $(0.23 \pm 0.20) \text{ g s}^{-1}$ ($r = 0.2 \text{ m}$), and $(0.48 \pm 0.41) \text{ g s}^{-1}$ ($r = 0.3 \text{ m}$) were calculated. Also, the model of Deutsch finds a useful match for the order of magnitude of \dot{m} compared with the results of the measurements (compare with Figures 5 and 6).

It is very hard to predict what a spill might look like in the case of real damage to an EFRT. This applies to both the roof and the retention area. In addition, for the retention area, it is possible to have spills on concrete or on a meadow, depending on the release event. If, in addition, the concrete or the meadow floor is warmed up by the solar radiation, the initial evaporation mass flow rates can be much higher than those specified here. Since neither release scenarios nor release quantities can be specified for general considerations, it is not necessary to use CFD models for an estimate of the initial mass flow. With regard to the roof, the spills are more likely to have a circular shape, but again the spill sizes are heavily dependent on hypothetical damages. In sum, with the lack of knowledge here, it seems sufficiently accurate to estimate \dot{m} with simplified models, if at least the order of magnitude is correct. The results of this work show that this is

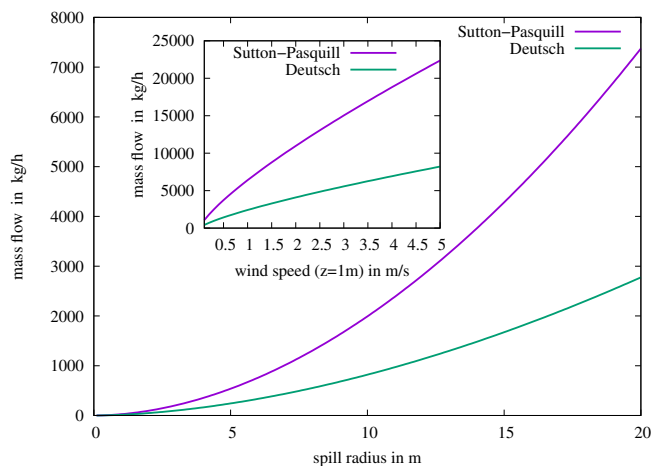


FIGURE 9 Illustration of the mass loss due to evaporation as a function of the spill radius calculated with the models of Sutton-Pasquill and Deutsch. The inset shows the mass loss due to evaporation as a function of the wind speed for a spill with a radius of $r = 20$ m ($p_d = 45 \times 10^3$ Pa, $T = 293$ K, and $\alpha = 0.25$) [Color figure can be viewed at wileyonlinelibrary.com]

possible with empirical spill evaporation models. With regard to the diameter of real EFRT, Figure 9 shows the size range of m depending on the diameter of the spill and for different wind speeds. Tanks for gasoline have a diameter in the range of 10–40 m, which is why the mass flow also for quite a big spills was estimated. In addition, uncertainties due to tolerances in the model input parameters were taken into account. As a conclusion of this work, it can be stated for accidents with spill formation that a determination of input mass flows with empirical spill evaporation models for CFD air dispersion studies are reasonable.

5 | SUMMARY

In this work, evaporation mass flow from gasoline spills were experimentally determined and compared with predictions of selected empirical models. Such spills have been considered because they can form as a consequence of various damage scenarios on floating roof tanks used for the storage of very large quantities of gasoline. Gasoline was selected here as a representative for a high vapor pressure refinery product. Preliminary studies show that, in the case of large spills, emissions are primarily relevant for the formation of hazardous explosive atmospheres. Therefore, the probability of occurrence of emission levels relevant for explosion protection strongly correlates with the formation probabilities of large spills. However, the aim of this work was not to determine as accurately as possible predictive values for the mass flow of vaporizing gasoline under very specific conditions but only to validate the actual expected orders of magnitude. For this purpose, figures have been given in this work, which illustrates the dependence of the evaporation mass flow between the size of the spill and for different environmental conditions. Experiments and empirical models were compared. This is to make the input

mass flows necessary for later CFD simulations plausible. It has also been shown that for a conservative, but not over-conservative estimate under various environmental conditions, the accuracy of empirical spill evaporation models is adequate. This justifies the coupling of CFD dispersion simulations and empirical spills evaporation models for the accuracy claim present in this project.

ACKNOWLEDGMENTS

The authors would like to thank the IBK Heyrothsberge for the opportunity to carry out the experiments there. We would also like to thank the meteorological Institute of the University of Hamburg for lending the sonic anemometer.

ORCID

Ronald Zinke  <https://orcid.org/0000-0002-7305-278X>

REFERENCES

- DIN EN 14015. Specification for the design and manufacture of site built, vertical, cylindrical, flat-bottomed, above ground, welded, steel tanks for the storage of liquids at ambient temperature and above; 2017.
- Imhof H. Aluminium domes under scrutiny. *Tank Storage*. 2011;7: 83–84.
- VDI. Emission Control, Marketing Installation Tank Farms (VDI 3479); 2010.
- API. MPMS Chapter 19-Evaporative Loss Measurement Section 2—Evaporative Loss From Floating-Roof Tanks; 1997.
- VDI. Emission control—Mineral Oil Refineries (VDI 2440); 2000.
- Zinke R, Köhler F, Krause U. Long-term emission measurements at a floating roof tank for gasoline storage. *J Loss Prev Process Ind*. 2018; 55:152–161.
- Köhler F, Zinke R. German Society for Petroleum and Coal, Science and Technology, DGMK Research Report 793: Explosive Gas Area Classifications at Storage Tanks, Hamburg, Germany; 2017.
- Lebuser U. Experimentelle und Theoretische Untersuchungen zur Verdunstung aus Flüssigkeitslachen [Dissertation]. Universität Dortmund; 1989.
- Deutsch S. Verdunstung aus Flüssigkeitslachen unter atmosphärischen Bedingungen, Universität Dortmund; 1995.
- Clancey JV. The evaporation and dispersion of flammable liquid spillages. Paper presented at: Chemical Process Hazards Conference; 1974; Manchester, UK.
- Mackay D, Matsugu RS. Evaporation rates of liquid hydrocarbon spills on land and water. *Can J Chem Eng*. 1973;51:434–439.
- Sutton OG. Wind structure and evaporation in a turbulent atmosphere. *Proc Royal Soc London, Series*. 1934;A146:701–722.
- Pasquill F. Evaporation from a plane, free liquid surface into a turbulent air stream. *Proc Royal Soc London, Series*. 1943;A182:75–95.
- Brighton PWM. Evaporation from a plane liquid surface into a turbulent boundary-layer. *J Fluid Mech*. 1985;159:323–345.
- Zhu L, Chen J, Liu Y, Geng R, Yu J. Experimental analysis of evaporation process for gasoline. *J Loss Prev Process Ind*. 2012;25: 916–922.
- Fingas MF. *Handbook of Oil Spill Science and Technology*. John Wiley & Sons; 2015.
- Okamoto K, Watanabe N, Hagimoto Y, Mia K, Ohtani H. Evaporation characteristics of multi-component liquid. *J Loss Prev Process Ind*. 2010;23:89–97.
- Okamoto K, Watanabe N, Hagimoto Y, Mia K, Ohtani H. Changes in evaporation rate and vapor pressure of gasoline with progress of evaporation. *Fire Saf J*. 2009;44:756–763.

19. Okamoto K, Hiramatsu M, Hino T, et al. Evaporation characteristics of ETBE-blended gasoline. *J Hazard Mater.* 2015;287:151-161.
20. Okamoto K, Hiramatsu M, Miyamoto H, et al. Evaporation and diffusion behaviour of fuel mixtures of gasoline and kerosene. *Fire Saf J.* 2012;49:47-61.
21. Hilpert M, Breyse PN. Infiltration and evaporation of small hydrocarbon spills at gas stations. *J Contam Hydrol.* 2014;170:39-52.
22. Mannan S, ed. *Lees' Loss Prevention in the Process Industries.* 4th ed. Elsevier; 2012.
23. Al Zubaidy I, Alsanea O, Ibrahim S, Saeed Y, Turki R, Alhammadi A. Diffusion coefficients of UAE gasoline as input to some environmental. *J Clean Energy Tech.* 2013;1:49-51.
24. Gesellschaft VDI. *VDI-Wärmeatlas. 10. Aufl. 2006. Wiesbaden.* Springer Berlin Heidelberg; 2005.
25. Wenck H, Schnieder C. *DGMK Forschungsbericht 509, Chemisch-physikalische daten von Otto-und Dieselmotoren, Deutsche Wissenschaftliche Gesellschaft für Erdöl.* Hamburg, Germany: Erdgas und Kohle e.V; 1993.
26. DIN 51754:1983-09 Prüfung flüssiger Brennstoffe; Bestimmung des Dampfdruckes nach Reid
27. ASTM D86-17. Standard Test Method for Distillation of Petroleum Products and Liquid Fuels at Atmospheric Pressure, Book of Standards Volume; 2007.
28. DIN EN 228: Kraftstoffe - Unverbleite Ottokraftstoffe - Anforderungen und Prüfverfahren; 2017.
29. Isidoro Matinez. Fuel Properties, Homepage polytechnische Universität Madrid (accessed on 04.2017).
30. Henley M, Letinski DJ, Carr J, Caro ML, Daughtrey W, White R. Health assessment of gasoline and fuel oxygenate vapors: generation and characterization of test materials. *Int Soc Regul Toxicol Pharmacol.* 2014;70:S13-S17.
31. CHEMIE.DE Information Service GmbH, Benzin. <http://www.chemie.de/lexikon/Benzin.html> (accessed on 04.2017)
32. KERN balance IKT 30K0.5. <https://www.kern-sohn.com>
33. Metek Sonic Anemometer USA-1. <https://metek.de/product/usonic-3-scientific/>
34. Institut für Brand-und Katastrophenschutz Heyrothsberge. <https://ibk-heyrothsberge.sachsen-anhalt.de>
35. Dräger X-am 7000. <https://www.draeger.com>

How to cite this article: Zinke R, Virothi N, Köhler F, Klippel A, Schalaus S, Krause U. Experimental measurement of initial evaporation mass flows from gasoline spills and comparison with empirical models. *Proc Safety Prog.* 2019;e12128. <https://doi.org/10.1002/prs.12128>